RPE **Radiation Physics & Engineering**
A Peer-Reviewed Journal
Published by K.N. Toosi University of Technology

http://rpe.kntu.ac.ir **Research Article**

Radiation Physics and Engineering 2026; ?(?):?–?

Monte Carlo optimization of collimator length for a parallel-hole prompt gamma camera in proton beam range verification

Sharareh Gharib, Payvand Taherparvar*

Department of Physics, Faculty of Science, University of Guilan, Rasht, Iran

HIGHLIGHTS

- Optimized collimator length for a parallel-hole prompt gamma camera in proton therapy using GATE code.
- Evaluated trade-off between detection sensitivity and spatial accuracy for collimator lengths of 4-8 cm.
- Spatial accuracy comparable to more complex slit- or pinhole-based systems.
- Demonstrates that sufficient count statistics are as critical as geometric resolution for clinical range verification.

ABSTRACT

This study aimed to optimize the collimator length for a parallel-hole prompt gamma camera dedicated to real-time proton beam range verification, achieving an optimal balance between detection sensitivity and spatial accuracy for clinical application. Comprehensive Monte Carlo simulations were conducted using the GATE platform with the QGSP_BIC_HP_EMZ physics list. A cylindrical PMMA phantom was irradiated with a 90 MeV monoenergetic proton beam, and a PG camera model consisting of an LSO scintillator coupled with a lead parallel-hole collimator was simulated. Collimator length was systematically varied from 4 to 8 cm, and detected PG events were analyzed within a 4.2-6.3 MeV energy window. System performance was evaluated using sensitivity (total detected counts) and spatial accuracy (Δ), defined as the absolute difference between true and reconstructed depth of maximum PG emission. The simulated energy spectrum exhibited characteristic photopeaks from carbon and oxygen, and a strong spatial correlation was confirmed between the distal edge of the Bragg peak and the PG emission maximum. Increasing collimator length decreased sensitivity but generally improved spatial accuracy. The optimal trade-off was achieved with a 7 cm collimator, yielding the best spatial accuracy of $\Delta = 2$ mm. This study identifies 7 cm as the optimal collimator length for a parallel-hole PG camera, achieving spatial accuracy comparable to more complex slit- or pinhole-based systems. The findings provide a quantitative design framework and underscore the critical importance of balancing geometric resolution with sufficient count statistics for precise and timely clinical range verification.

KEYWORDS
Proton therapy
Prompt gamma imaging
Range verification
Monte Carlo simulation
Collimator optimization
GATE simulation

HISTORY
Received:
Revised:
Accepted:
Published:

1 Introduction

Proton therapy provides superior dose conformity compared to conventional photon radiotherapy owing to the Bragg peak, which enables protons to deposit the majority of their energy at a well-defined depth, thus sparing surrounding healthy tissue (Wilson, 1946). However, uncertainties in the in vivo proton range-caused by anatomical variations, setup errors, and limitations in converting CT data to stopping power-force the use of conservative safety margins that partially negate this advantage (Idrissi et al., 2024; Perali et al., 2014). Real-time in vivo range verification is therefore essential.

Positron emission tomography (PET) has been investigated for this purpose, but its reliance on slow decay, biological washout, and post-irradiation acquisition limits immediate feedback (Dendooven et al., 2015; Zarifi et al., 2019). Prompt gamma (PG) imaging overcomes these limitations because PG rays are emitted within nanoseconds of nuclear de-excitation, are temporally correlated with dose deposition, and their distal fall-off is strongly correlated with the proton range (Moteabbed et al., 2011; Bom et al., 2012; JW., 2009; Priegnitz et al., 2015).

Several collimation strategies have been explored. Min

*Corresponding author: p.taherparvar@gmail.com

https://doi.org/

et al. (2006) provided the first experimental demonstration that a single-hole collimator with a CsI(Tl) scintillator could locate the dose falloff within 1-2 mm and proposed extending the approach to multi-parallel-hole cameras. Smeets et al. (Smeets et al., 2012) developed a knife-edge slit camera that achieved 1-2 mm standard deviation in range estimation at clinical doses. Wang et al. (Wang et al., 2018) introduced a pixelated PG detector based on a parallel-hole collimator (grated shielding) and demonstrated its feasibility with FLUKA simulations, though without systematic optimization of the collimator. Park et al. (Park et al., 2019) designed a multi-slit camera that directly extracted the distal dose fall-off with an accuracy of 2-3 mm, and Son et al. (Son et al., 2025) simulated a pinhole-collimated SPECT system that matched the reconstructed PG peak to the true emission peak within ~ 1 mm.

Monte Carlo (MC) simulations are essential for PG system design, as they accurately model PG production, transport, and detector response, and enable systematic variation of parameters such as detector configuration and collimator geometry (Jan et al., 2004). Despite notable progress, the systematic optimization of a parallelhole collimator-specifically the tradeoff between detection sensitivity and spatial accuracy at a clinically relevant proton energy-has not been addressed. In particular, the influence of collimator length on the performance of a parallel-hole PG camera has not been quantitatively investigated. The present study directly addresses this gap. Using the GATE Monte Carlo platform, a PG camera equipped with a lead parallelhole collimator is simulated for a 90 MeV proton beam incident on a PMMA phantom, and the collimator length is systematically varied from 4 to 8 cm. The primary objective is twofold: (i) to characterize the PG emission profile and (ii) to identify the collimator length that yields the optimal compromise between detection sensitivity (total counts in the 4.2-6.3 MeV window) and spatial accuracy (Δ, the absolute difference between the true and reconstructed depth of the PG emission maximum). To our knowledge, this is the first study that systematically optimizes the parallelhole collimator length for PGbased proton range verification through a quantitative sensitivity-accuracy tradeoff analysis. The results provide a clear design framework for a mechanically simple, compact, and clinically practical PG camera prototype.

2 Material and Methods

2.1 Simulation Framework

A comprehensive Monte Carlo simulation study was performed using the GATE/Geant4 simulation platform (Jan et al., 2004), a toolkit widely employed in medical imaging (Taherparvar and Sadremomtaz, 2018) and radiotherapy research (Taherparvar and Fardi, 2021; Gharib and Taherparvar, 2025). All simulations utilized the QGSP_BIC_HP_EMZ physics list, which is specifically recommended for hadron therapy applications due to its accurate modeling of hadronic interactions and secondary particle production. Within the phantom, the production threshold (range cut) for secondary particles was set to 0.1 mm to ensure submillimeter accuracy in the depth-dose and PG emission profiles, while a 1 mm threshold was applied in the surrounding world volume to reduce computation time. The simulation setup was further validated by comparing the position of the Bragg peak in water with standard reference data. A cylindrical water phantom with the same dimensions as the PMMA phantom was irradiated with a monoenergetic proton beam of 90 MeV. The depth of the Bragg peak (i.e., the depth of maximum dose deposition) was extracted from the longitudinal dose profile and compared with the corresponding value tabulated by the ICRU (Report 49) for water. The simulated Bragg peak position agreed with the ICRU data within 2%, confirming the accuracy of the physics models employed for proton transport and dose deposition. To ensure high statistical precision for the analysis of PG emission and detection, a total of 2×10^9 primary proton histories were simulated for each investigated configuration.

2.2 Phantom and Irradiation Setup

A cylindrical, homogeneous phantom of polymethyl methacrylate (PMMA) with a diameter of 3.8 cm and a height of 29 cm was modeled. PMMA was chosen as the phantom material because its elemental composition ($C_5H_8O_2$) and mass density ($\sim 1.19\,\mathrm{g.cm^{-3}}$) closely mimic soft tissue, while its carbon and oxygen content yields the characteristic prompt gamma lines at 4.44, 5.24, and 6.13 MeV that are central to PG-based range verification. Moreover, PMMA is a well-established tissue substitute in proton therapy research, facilitating comparison with previously published studies.

The phantom's central axis was aligned with the beam direction (z-axis). For detailed depth-dose and depth-emission analysis, the phantom was virtually segmented into 290 axial slices, each 1 mm thick. The phantom was irradiated with a monoenergetic proton beam of 90 MeV, with a cylindrical crosssection of 2.5 mm radius and no angular divergence (parallel beam). This energy is primarily suited for the treatment of tumors situated at shallow depths.

2.3 PG Camera Design and Simulation

A dedicated PG-ray camera was modeled to evaluate the impact of collimator geometry on the range verification of proton beam. The schematic configuration of the camera is depicted in Fig. 1, with its main components consisting of a crystal and a collimator. The detector consisted of a monolithic block of Lutetium Oxyorthosilicate (LSO) with a thickness of 3 cm. For fine-grained data collection, the crystal was modeled with a pixelated structure of $400(x) \times 90(y)$ elements, each 1×1 mm^2 in cross-section. A parallel-hole collimator made of lead was placed in front of the crystal. The collimator had a fixed pattern of 40×9 square holes (9×9 mm^2 each, 3 mm septal thickness). The collimator length was the primary variable parameter, with five values simulated: 4, 5, 6, 7, and 8 cm.

This range was selected based on preliminary scoping simulations and practical considerations: collimator lengths shorter than 4 cm resulted in insufficient spatial resolution ($\Delta > 5$ mm), while lengths exceeding 8 cm led to a severe reduction in detected counts, degrading statistical precision in peak localization. Additionally, the selected interval corresponds to approximately 2-4 mean free paths of lead for the dominant PG photons in the 4.2-6.3 MeV energy window, ensuring effective attenuation of non-parallel incident photons while preserving adequate system sensitivity. The upper bound also accounts for the mechanical constraints of a compact camera design intended for future clinical integration. The simulated PG camera represents a purely hypothetical conceptual design intended to guide future prototype development; it is not based on an existing physical system. The 3 cm thick LSO crystal was selected for its high stopping power for 4-6 MeV photons, offering a practical trade-off between detection efficiency and spatial resolution. The 40×9 square-hole lead collimator (9×9 mm^2 holes, 3 mm septal walls) provides sufficient axial field of view to cover the expected PG emission region while maintaining acceptable septal penetration at the relevant energies. The camera was positioned laterally to the phantom to detect PG rays emitted perpendicular to the beam axis.

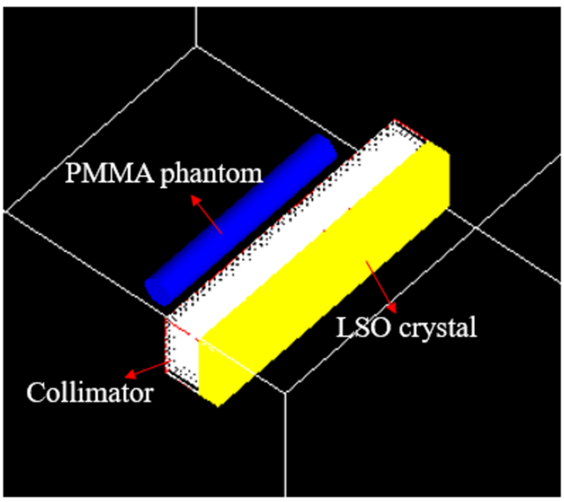

Figure 1: Schematic of the simulated PG camera.

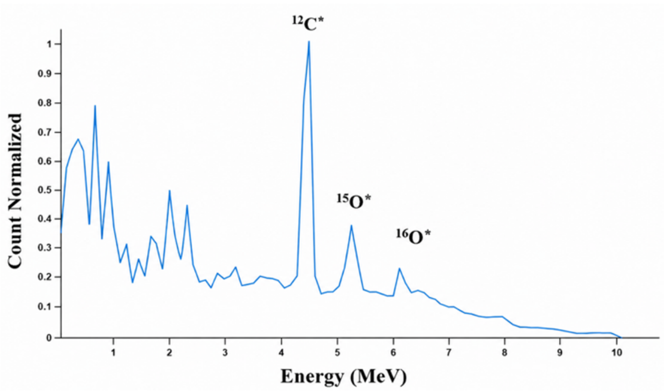

Figure 2: Simulated PG-ray energy spectrum from proton interactions in the PMMA phantom.

2.4 *Data Acquisition and Analysis*

Spatial distribution data of the detected PGs along the beam axis (z-axis) were recorded for each collimator configuration. All analyzed events were filtered within a broad energy window from 4.2 MeV to 6.3 MeV. This window encompasses the dominant PG-ray lines from nuclear de-excitation of Carbon and Oxygen in PMMA. The one-dimensional spatial profile (counts vs. depth) of the detected PGs was fitted with a Gaussian function. The centroid of this fitted peak was taken as the reconstructed depth of the PG emission maximum. For performance metrics analysis: two key figures of merit were evaluated:

1. System Sensitivity: Defined as the total number of PG-ray counts detected within the 4.2-6.3 MeV window.

2. Spatial Accuracy (Δ): Calculated as the absolute difference between the true axial depth of the maximum PG emission (directly extracted from the phantom slice data) and the reconstructed depth obtained from the Gaussian fit of the camera data. Finally, the optimal collimator length was identified by analyzing the trade-off curve between system sensitivity (expected to decrease with longer collimators) and spatial accuracy, Δ (expected to improve with longer collimators).

3 Results

3.1 *PG-ray Energy Spectrum*

The simulated PG-ray energy spectrum resulting from proton interactions within the PMMA phantom is presented in Fig. 2. Three prominent photopeaks were identified, corresponding to characteristic gamma-ray lines from de-exciting nuclei: the 4.44 MeV line from excited Carbon-12 (^{12}C*), the 5.24 MeV line from excited Oxygen-15 (^{15}O*), and the 6.13 MeV line from excited Oxygen-16 (^{16}O*). In accordance with established methodology (Zarifi et al., 2017), a broad energy window from 4.2 MeV to 6.3 MeV was selected for subsequent analysis. This window encompasses all three major peaks, thereby maximizing the signal relevant for proton range verification.

3.2 *Correlation of the Bragg Peak and PG Emission*

The axial depth-dose distribution (Bragg curve) and the corresponding PG-ray emission profile are shown in Fig. 3. A strong spatial correlation is observed between the distal edge of the dose fall-off and the maximum of the PG emission. The simulation results indicate that the Bragg peak maximum occurs at a depth of 54 mm (corresponding to -91 mm relative to the phantom center), while the peak of the PG-ray emission profile is located at a depth of 44 mm (corresponding to -101 mm relative to the phantom center). This shift is consistent with the physical origin of PGs from nuclear interactions occurring along the proton track before it comes to rest.

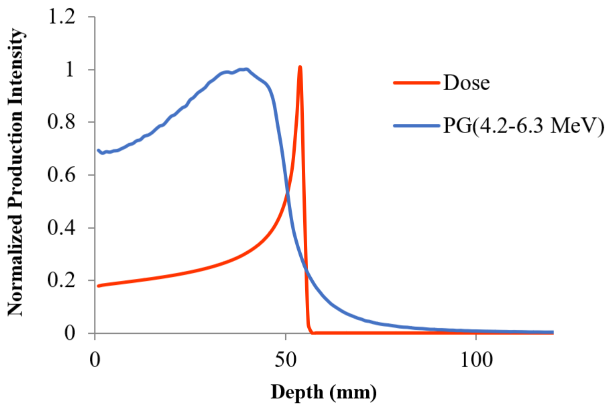

Figure 3: Axial depth profiles: dose deposition (Bragg curve, red) and PG-ray emission (blue).

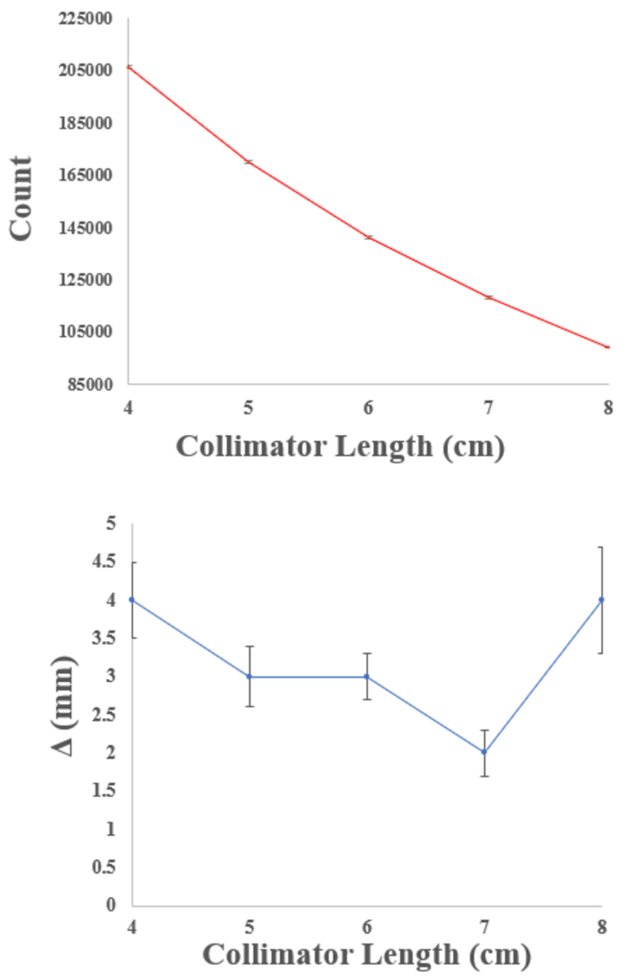

Figure 4: Trade-off curve between System Sensitivity (top chart, counts) and Spatial Accuracy, Δ (bottom chart, mm) as a function of collimator length. Error bars for sensitivity represent the Poisson counting uncertainty ($\pm\sqrt{N}$). Error bars for Δ indicate the standard deviation of the Gaussian centroid obtained from the fit to the PG depth profile.

3.3 Optimization of Collimator Length

The impact of collimator length on system performance for lengths ranging from 4 to 8 cm is presented in Fig. 4. As expected, the detected count rate decreases monotonically with increasing collimator length due to the reduction in geometric acceptance. In contrast, spatial accuracy (Δ) generally improves with increasing collimator length as a result of enhanced geometric collimation. However, for a collimator length of 8 cm, the substantial reduction in detected counts leads to increased statistical uncertainty in peak localization, ultimately degrading the effective spatial accuracy.

For quantitative analysis, Gaussian fitting was performed on the PG depth profiles corresponding to all investigated collimator lengths, and the associated Δ values were extracted. The results indicate that the optimal balance between detection sensitivity and spatial accuracy is achieved with a collimator length of 7 cm. This configuration yields the minimum Δ value (2 mm). At a collimator length of 8 cm, the detected PG counts dropped substantially, which increased the statistical noise in the depth profile. This degraded the stability of the Gaussian fit: the uncertainty on the fitted peak position became larger, as indicated by the wider error bar on Δ, and a slight systematic shift of the centroid occurred. As a result, Δ increased, showing that beyond the optimal length the benefit of improved geometric resolution is offset by the loss in count statistics. Hence, 7 cm provides the best tradeoff between sensitivity and spatial accuracy. Figure 5 shows the fitted PG depth profile for this optimal collimator.

3.4 PG Projections

Figure 6 shows the projections of the detected PG distributions along the beam axis for all investigated collimator lengths (4-8 cm). These profiles clearly illustrate the trade-off between resolution and sensitivity. The figures demonstrate an inverse relationship between collimator length and photon count, indicating that increasing the collimator length results in a reduction in the number of detected photons. The dark bands visible in the 2D projections of Fig. 6 correspond to the shadows of the collimator septa cast onto the pixelated detector. Because the collimator holes (9×9 mm^2) are separated by 3 mm thick lead septa, the regions directly behind the septa receive no primary photons from the phantom, creating a characteristic pattern of dark lines. As the collimator length increases, the geometric acceptance angle of each hole narrows, reducing the detector area illuminated by a given source point and thereby widening the nonilluminated septal shadows. This effect explains the observed broadening of the dark lines with increasing collimator length.

4 Discussion

This study successfully demonstrated the systematic optimization of a parallel-hole collimator for a PG camera dedicated to proton beam range verification using Monte Carlo simulations, identifying a collimator length of 7 cm as a potentially optimal design parameter. The observed spatial correlation between the PG emission peak and the distal edge of the Bragg peak–with the PG peak occurring at a shallower depth- is a well-documented precursor signal for range estimation, as demonstrated in previous studies (Min et al., 2006; Testa et al., 2010). This shift is consistent with the physical origin of PGs, which are generated by nuclear interactions along the proton track before it stops. Furthermore, the simulated energy spectrum revealed characteristic photopeaks corresponding to de-excitation of carbon-12 (4.44 MeV), oxygen-15 (5.24 MeV), and oxygen-16 (6.13 MeV) nuclei, matching prior spectral reports for PMMA (Zarifi et al., 2017).

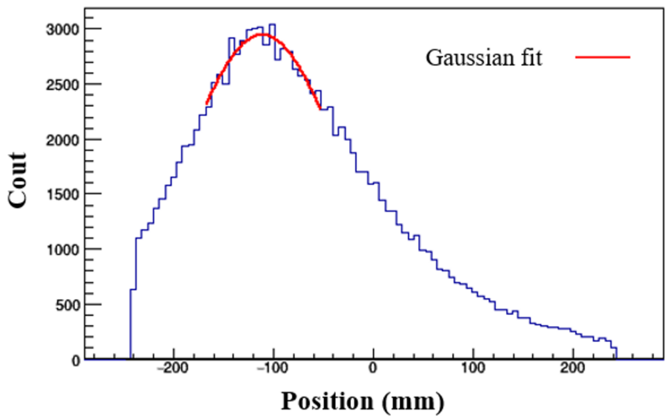

Figure 5: PG depth profile and Gaussian fit for the optimal collimator length of 7 cm, yielding the best spatial accuracy $\Delta = 2$ mm.

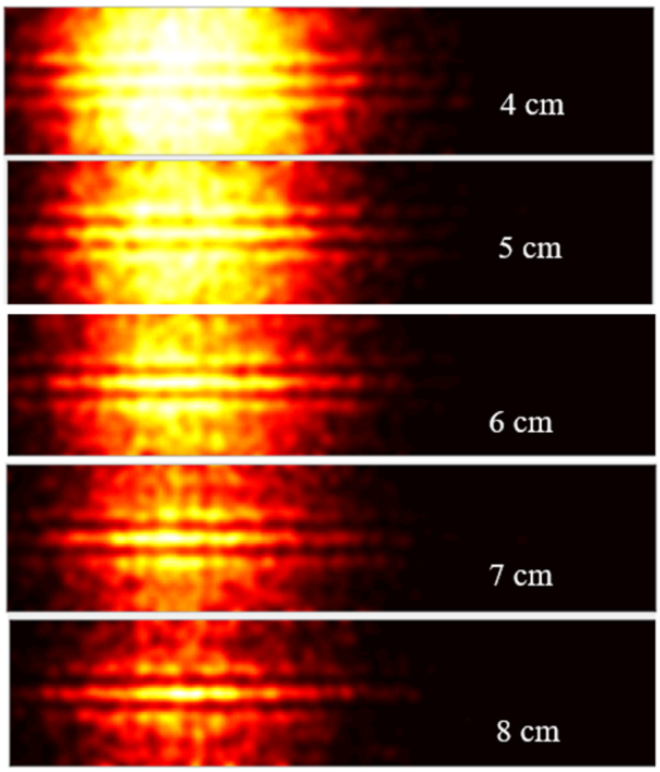

Figure 6: Projections of detected PG rays for all investigated collimator lengths (4-8 cm).

Our results demonstrate a spatial accuracy of 2 mm, a key finding of this study. A comparison of the spatial accuracy achieved in this study with values reported for alternative collimation approaches confirms the competitiveness of the optimized parallel-hole design. Early measurements by Min et al. (Min et al., 2006), using a single-hole collimator and a CsI(Tl) scintillator, experimentally demonstrated that prompt gamma detection could locate the dose falloff region within 1-2 mm. The knife-edge slit camera of Smeets et al. (Smeets et al., 2012) achieved a standard deviation of 1-2 mm on range estimation in a homogeneous PMMA target for clinically relevant proton numbers at 100 and 160 MeV. The multi-slit camera of Park et al. (Park et al., 2019), tested with therapeutic proton beams of 95-186 MeV, located the 90% distal dose falloff with an error of 2-3 mm for spots containing at least 3.8×10^8 protons. A recent simulation study by Son et al. (Son et al., 2025) based on a pinhole-collimated SPECT system demonstrated that the reconstructed prompt gamma peak matched the simulated emission peak within approximately 1 mm for proton energies of 80-120 MeV when imaging the 4.4 MeV line. In the present work, the parallel-hole camera with a collimator length of 7 cm yields a spatial accuracy of $\Delta = 2$ mm, defined as the absolute difference between the true and reconstructed depth of maximum prompt gamma emission. This value falls well within the 13 mm range reported for more complex slit- and pinhole-based systems, indicating that a properly optimized parallel-hole configuration can provide comparable range verification accuracy while offering inherent mechanical simplicity.

The quantified trade-off curve between system sensitivity and spatial accuracy provides crucial engineering insight. As expected, increasing collimator length improved geometric resolution and reduced Δ, but concurrently decreased the total detected counts due to reduced geometric acceptance. The optimum was found at 7 cm, where the spatial accuracy (Δ) reached its minimum value, indicating the best performance. The performance degradation observed for the 8 cm collimator despite its greater length underscores a critical point: maximizing geometric resolution alone can be counterproductive if the count rate becomes too low for statistically precise peak localization within clinically feasible timeframes. This conclusion is particularly relevant for clinical translation, where range verification must be performed under time constraints and amidst inherently low PG yield.

5 Conclusions

In this study, we determined an optimal collimator length for a parallel-hole PG camera dedicated to proton beam range verification. By quantitatively evaluating the intrinsic trade-off between detection sensitivity and spatial accuracy, a collimator length of 7 cm was identified as providing the best performance compromise. This design achieved a spatial accuracy of 2 mm, a result competitive with more complex slit or pinhole-based systems reported in the literature.

The work confirms the fundamental spatial correlation between the distal fall-off of the PG emission and the proton Bragg peak, underscoring the physical basis for this verification technique. More importantly, it provides a crucial, quantitative engineering guideline: maximizing geometric resolution must be balanced against the necessity for sufficient detected counts to ensure statistically robust and timely measurement in a clinical setting.

Conflict of Interest

The authors declare no potential conflict of interest regarding the publication of this work.

Funding

The authors declare that no funds, grants, or other financial support were received during the preparation of this manuscript.

References

Bom, V., Joulaeizadeh, L., and Beekman, F. (2012). Real-time prompt gamma monitoring in spot-scanning proton therapy using imaging through a knife-edge-shaped slit. *Physics in Medicine and Biology*, 57(2):297–308.

Dendooven, P., Buitenhuis, H., Diblen, F., et al. (2015). Short-lived positron emitters in beam-on PET imaging during proton therapy. *Physics in Medicine & Biology*, 60(23):8923–8947.

Gharib, S. and Taherparvar, P. (2025). Evaluation of the distribution of prompt gammas emission during proton therapy using the GATE Monte Carlo toolkit. *Journal of Radiation Safety and Measurement*, 13(4):191–202.

Idrissi, A. B., Borghi, G., Caracciolo, A., et al. (2024). First experimental verification of prompt gamma imaging with carbon ion irradiation. *Scientific Reports*, 14(1):25750.

Jan, S., Santin, G., Strul, D., et al. (2004). GATE: a simulation toolkit for PET and SPECT. *Physics in Medicine & Biology*, 49(19):4543–4561.

JW., K. (2009). Pinhole camera measurements of prompt gamma-rays for detection of beam range variation in proton therapy. *Journal of the Korean Physical Society*, pages 1673–1676.

Min, C.-H., Kim, C. H., Youn, M.-Y., et al. (2006). Prompt gamma measurements for locating the dose falloff region in the proton therapy. *Applied physics letters*, 89(18).

Moteabbed, M., España, S., and Paganetti, H. (2011). Monte Carlo patient study on the comparison of prompt gamma and PET imaging for range verification in proton therapy. *Physics in Medicine & Biology*, 56(4):1063–1082.

Park, J. H., Kim, S. H., Ku, Y., et al. (2019). Multi-slit prompt-gamma camera for locating of distal dose falloff in proton therapy. *Nuclear Engineering and Technology*, 51(5):1406–1416.

Perali, I., Celani, A., Bombelli, L., et al. (2014). Prompt gamma imaging of proton pencil beams at clinical dose rate. *Physics in Medicine & Biology*, 59(19):5849–5871.

Priegnitz, M., Helmbrecht, S., Janssens, G., et al. (2015). Measurement of prompt gamma profiles in inhomogeneous targets with a knife-edge slit camera during proton irradiation. *Physics in Medicine & Biology*, 60(12):4849–4871.

Smeets, J., Roellinghoff, F., Prieels, D., et al. (2012). Prompt gamma imaging with a slit camera for real-time range control in proton therapy. *Physics in Medicine and Biology*, 57(11):3371–3405.

Son, J., Oh, G., Lee, J., et al. (2025). Prompt-gamma tomographic imaging for range verification in pencil beam-scanning proton therapy. *Journal of Instrumentation*, 20(06):P06030.

Taherparvar, P. and Fardi, Z. (2021). Development of GATE Monte Carlo Code for Simulation and Dosimetry of New I-125 Seeds in Eye Plaque Brachytherapy. *Nuclear Medicine and Molecular Imaging*, 55(2):86–95.

Taherparvar, P. and Sadremomtaz, A. (2018). Development of GATE Monte Carlo simulation for a CsI pixelated gamma camera dedicated to high resolution animal SPECT. *Australasian Physical & Engineering Sciences in Medicine*, 41(1):31–39.

Testa, M., Bajard, M., Chevallier, M., et al. (2010). Real-time monitoring of the bragg-peak position in ion therapy by means of single photon detection. *Radiation and Environmental Biophysics*, 49(3):337–343.

Wang, J.-L., Cruz, L. A., and Lu, M. (2018). Pixelated prompt gamma imaging detector for online measurement of proton beam: Monte Carlo feasibility study by FLUKA. *Radiation Detection Technology and Methods*, 2(1):4.

Wilson, R. R. (1946). Radiological use of fast protons. *Radiology*, 47(5):487–491.

Zarifi, M., Guatelli, S., Bolst, D., et al. (2017). Characterization of prompt gamma-ray emission with respect to the Bragg peak for proton beam range verification: A Monte Carlo study. *Physica Medica*, 33:197–206.

Zarifi, M., Guatelli, S., Qi, Y., et al. (2019). Characterization of prompt gamma ray emission for in vivo range verification in particle therapy: A simulation study. *Physica Medica*, 62:20–32.

To cite this article:

Sh. Gharib, P. Taherparvar. Monte Carlo optimization of collimator length for a parallel-hole prompt gamma camera in proton beam range verification. *Radiation Physics and Engineering*, In Press.

DOI:

To link to this article: